

RESEARCH

Open Access



AiGPro: a multi-tasks model for profiling of GPCRs for agonist and antagonist

Rahul Brahma¹, Sunghyun Moon¹, Jae-Min Shin^{2*} and Kwang-Hwi Cho^{1*}

Abstract G protein-coupled receptors (GPCRs) play vital roles in various physiological processes, making them attractive drug discovery targets. Meanwhile, deep learning techniques have revolutionized drug discovery by facilitating efficient tools for expediting the identification and optimization of ligands. However, existing models for the GPCRs often focus on single-target or a small subset of GPCRs or employ binary classification, constraining their applicability for high throughput virtual screening. To address these issues, we introduce AiGPro, a novel multitask model designed to predict small molecule agonists (EC₅₀) and antagonists (IC₅₀) across the 231 human GPCRs, making it a first-in-class solution for large-scale GPCR profiling.

Leveraging multi-scale context aggregation and bidirectional multi-head cross-attention mechanisms, our approach demonstrates that ensemble models may not be necessary for predicting complex GPCR states and small molecule interactions. Through extensive validation using stratified tenfold cross-validation, AiGPro achieves robust performance with Pearson's correlation coefficient of 0.91, indicating broad generalizability. This breakthrough sets a new standard in the GPCR studies, outperforming previous studies. Moreover, our first-in-class multi-tasking model can predict agonist and antagonist activities across a wide range of GPCRs, offering a comprehensive perspective on ligand bioactivity within this diverse superfamily. To facilitate easy accessibility, we have deployed a web-based platform for model access at <https://aicadd.ssu.ac.kr/AiGPro>.

Scientific Contribution We introduce a deep learning-based multi-task model to generalize the agonist and antagonist bioactivity prediction for GPCRs accurately. The model is implemented on a user-friendly web server to facilitate rapid screening of small-molecule libraries, expediting GPCR-targeted drug discovery. Covering a diverse set of 231 GPCR targets, the platform delivers a robust, scalable solution for advancing GPCR-focused therapeutic development.

The proposed framework incorporates an innovative dual-label prediction strategy, enabling the simultaneous classification of molecules as agonists, antagonists, or both. Each prediction is further accompanied by a confidence score, offering a quantitative measure of activity likelihood. This advancement moves beyond conventional models focusing solely on binding affinity, providing a more comprehensive understanding of ligand-receptor interactions.

At the core of our model lies the Bi-Directional Multi-Head Cross-Attention (BMCA) module, a novel architecture that captures forward and backward contextual embeddings of protein and ligand features. By leveraging BMCA, the model effectively integrates structural and sequence-level information, ensuring a precise representation of molecular interactions. Results show that this approach is highly accurate in binding affinity predictions and consistent across diverse GPCR families.

*Correspondence:

Jae-Min Shin
jmshin@azothbio.com
Kwang-Hwi Cho
chokh@ssu.ac.kr

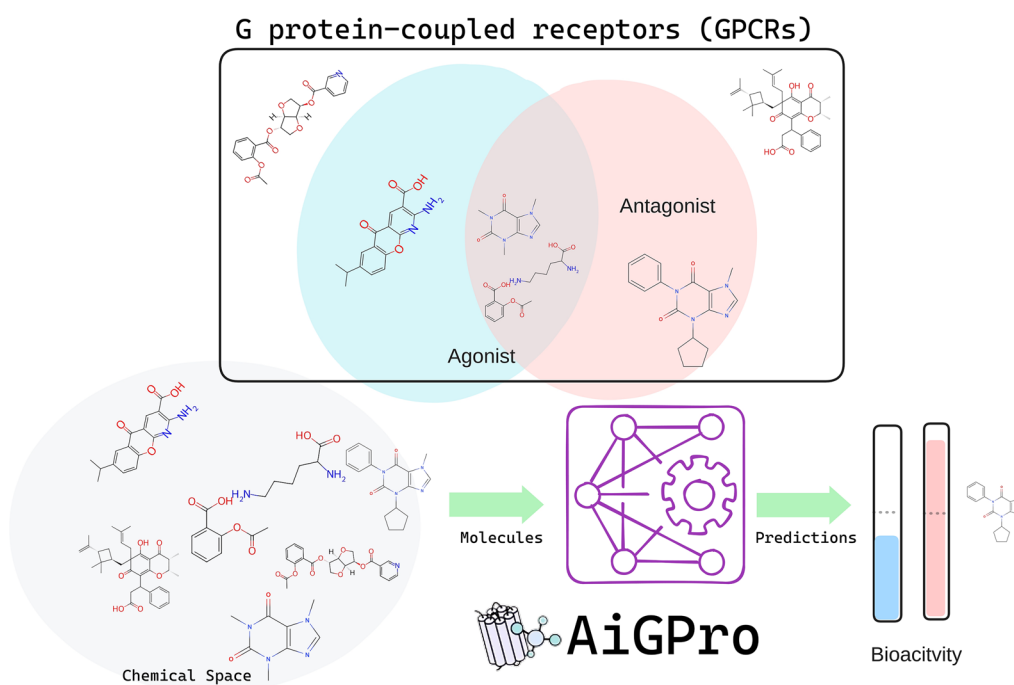


© The Author(s) 2025. **Open Access** This article is licensed under a Creative Commons Attribution-NonCommercial-NoDerivatives 4.0 International License, which permits any non-commercial use, sharing, distribution and reproduction in any medium or format, as long as you give appropriate credit to the original author(s) and the source, provide a link to the Creative Commons licence, and indicate if you modified the licensed material. You do not have permission under this licence to share adapted material derived from this article or parts of it. The images or other third party material in this article are included in the article's Creative Commons licence, unless indicated otherwise in a credit line to the material. If material is not included in the article's Creative Commons licence and your intended use is not permitted by statutory regulation or exceeds the permitted use, you will need to obtain permission directly from the copyright holder. To view a copy of this licence, visit <http://creativecommons.org/licenses/by-nc-nd/4.0/>.

By unifying agonist and antagonist bioactivity prediction into a single model architecture, we bridge a critical gap in GPCR modeling. This enhances prediction accuracy and accelerates virtual screening workflows, offering a valuable and innovative solution for advancing GPCR-targeted drug discovery.

Keywords Artificial intelligence, GPCR, Agonist and antagonist, Machine learning, Drug development

Graphical Abstract



Introduction

G-protein coupled receptors (GPCRs) are a vast family of transmembrane proteins that play a critical role in numerous cellular signaling. They facilitate the transmission of signals from outside the cell to the inside by regulating G proteins. They are involved in multiple signaling pathways activated by various chemical compounds, hormones, and neurotransmitters, influencing crucial cellular processes such as growth, differentiation, vision, olfaction, and gustatory [1]. Out of the 826 human GPCRs, approximately 350 non-olfactory members are considered druggable, with 165 validated as drug targets [2]. Given their critical role in fundamental physiological functions, it is not surprising that they are associated with neurodegenerative and psychiatric disorders, such as Parkinson's and Alzheimer's disease (AD) [2]. Despite challenges in drug development for Alzheimer's, clinical trials exploring GPCR agonism in treatment are underway [3, 4]. The human GPCR family is categorized into

classes A (rhodopsin), B (secretin and adhesion), C (glutamate), and F (Frizzled) subfamilies based on amino acid sequences. Notably, approved drugs for neuropsychiatric diseases mainly target class A and C GPCRs, underscoring their significance in therapeutic strategies. Understanding and targeting specific GPCR classes offer potential breakthroughs in treating complex neurological conditions. Remarkably, one-third of currently available drugs target GPCRs, addressing a spectrum of human diseases, including cardiac malfunction, obesity, asthma, and migraines. GPCRs account for 12% of all human protein drug targets and contribute to the therapeutic effects of 34% of small molecule drugs [2, 5, 6]. Certain drugs, exemplified by clozapine, initially designed for specific protein targets, have been retrospectively demonstrated to exert clinical actions by modulating multiple GPCR proteins [7–9]. This underscores the unique polypharmacological profiles associated with GPCR modulation.

As of Dec 2023, it was reported that approximately 35% (approximately 700 drugs) of all US FDA-approved drugs act on GPCR targets [6, 10]. Furthermore, 321 drugs targeting GPCRs are currently in clinical trials, 66 of which target GPCRs not presently targeted by approved drugs. Examples of drugs in clinical trials include LJPC-501, INT-767, and RX-10045 [5]. Between 2011 and 2015, drugs that target GPCRs generated over \$900 billion in sales [11]. Collectively, GPCRs, along with related proteins upstream or downstream from GPCRs, constitute approximately 17% of all protein targets for approved drugs [6]. It accounts for about 12% of this, underscoring its vital role in drug development and therapeutic interventions [6]. This emphasizes the significance of GPCRs as critical players in pharmaceutical research and treatment modalities.

The structural elucidation of GPCRs began in 2000 with the resolution of bovine rhodopsin, marking a continuous increase in experimental GPCR structures. Despite progress, only 70 unique GPCRs have been characterized among 370 GPCR-ligand complexes with resolved structures [12]. Among these structures, 25 GPCRs have both agonist and antagonist binding, 33 exclusively with antagonist binding, 11 solely with agonist binding, and one without any ligand bound, providing a detailed overview of GPCR conformational diversity [12]. The scarcity of high-resolution GPCR structures challenges understanding activation mechanisms and hinders structure-based drug design [13]. Experimental efforts and computational advancements like molecular dynamics (MD) and machine learning (ML) have produced high-quality models systematically cataloged in repositories such as GPCRdb [14, 15] and GPCR-EXP [16]. However, many GPCRs still lack experimental 3D data. In the absence of receptor structures, alternative ligand-based techniques, such as quantitative structure–activity relationship (QSAR) models, have been explored [17]. Datasets detailing small-molecule activity against GPCRs offer opportunities for *in silico* ligand-based screening, including the application of ML models.

Recent advancements in computational approaches have significantly contributed to understanding protein interactions with ligands [18–23]. Several classification models have been developed to discern the activity of GPCR ligands, ranging from simple binary prediction like active/inactive or predicting bioactivity of antagonist/agonist on a single GPCR to a small subset of GPCRs. One classification model was developed using hub and cycle structures of ligands, along with the amino acid motif sequence of GPCRs [24]. Based on the UniProt and the Database of Interacting Proteins (DIP), a Random Forest (RF) model was developed with a focus on specific and important types of GPCRs

and employed different types of sequence-based features to improve the accuracy of the predictions [25]. The Helix encoder, a compound-protein interaction (CPI) model explicitly designed for class A GPCRs, employs attention-based convolutional neural networks (CNNs) [26]. GPCRLigNet, on the other hand, is an ML-based feed-forward neural (FFN) network incorporating dilated graph convolutional networks (GCN) trained with a diverse dataset to conduct binary classification into active and active GPCR ligands [27]. DeepREAL employs a multi-scale modeling approach to analyze genome-wide ligand-induced receptor activities through transfer learning from a pre-trained binary interaction classification model [28]. SDTNBI, or Substructure-Drug-Target Network-Based Inference, prioritizes potential targets for old drugs, failed drugs, and new chemical entities by integrating network analysis and chemoinformatics to bridge the gap between novel chemical entities and the established Drug-Target Interaction (DTI) network [29]. A two-step RF-based binary classifier also performed similarly to SDTNBI with an AUC of 0.795 [30]. DTI-MLCD innovatively transforms DTI prediction from binary to multi-label classification, incorporating community detection for label correlations using a fast greedy algorithm [31]. It adapts feature representations based on dataset-specific requirements, achieving competitive performance while addressing computational load and label correlation issues inherent in binary methods [31]. Some studies have focused on a specific target; for instance, in [32], an RF model was developed to classify ligands based on molecular fingerprint features against Human Adenosine Receptor type 2A (A_{2A}R), which is implicated in neurodegenerative diseases like Parkinson's and cancer and is a proven druggable target [32–34]. Docking and ML were also used to identify the pharmacological activity of ligands for the β_2 adrenergic receptor, focusing on the specific residues for both agonist and antagonist ligands interaction [35]. However, another focus was on analyzing the features of a ligand by utilizing molecular fingerprints and embeddings for GPR151, utilizing numerous classical feature selection algorithms and DL models [36]. However, the interaction of compounds with GPCR is more complex than binary or two mutually exclusive classes, i.e., Agonist or Antagonist. Other subtle activity classes include neutral antagonists, both agonists and antagonists, inverse and partial agonists, etc. A multi-class model could be a more suitable choice; however, the need for such clean labeled data makes it a challenging problem. In practice, detecting if an unseen ligand is in its state of activity, i.e., a regression model for both agonist and antagonist, would be more helpful. More relevant

efforts are screening Lasso of ECFPs and the deep neural nets (SED) approach, comprising ECFP generation, critical substructure selection, and bioactivity prediction using a DNN regression model [37]. This method was applied to 16 GPCRs (Classes A, B, C, and F, spanning 13 subfamilies). Further, they also used weighted DL and RF with five types of molecular fingerprints to develop the WDL-RF methods, which extended to 26 GPCRs, covering the same classes as their previous article [38]. GCN has also effectively predicted bioactivity against diverse targets, including 33 GPCRs [39]. Further, pdCSM-GPCR, another graph-based model, predicts bioactivity across 36 primary GPCR targets [40]. Recently, ensemble models employing five algorithms demonstrated a robust predictive capability for EC₅₀ values of human orphan GPCRs, achieving a Pearson's correlation coefficient of 0.85 through training on 200 GPCRs utilizing MSA, physicochemical properties, and molecular fingerprints [41].

Despite extensive efforts in GPCR research, current methodologies predominantly center on classifying active and inactive or characterizing agonist and antagonist attributes, limiting comprehensive small molecule profiling against GPCRs, especially regarding bioactivity properties. Existing models for regression tasks are scarce and

often focus on a limited GPCR subset, underscoring the complexities in accurately predicting bioactivity for small molecules against GPCRs. This gap requires a more comprehensive approach to deciphering the complexities of GPCR interactions.

Recently, the application of attention-based models, proven highly successful in natural language processing (NLP) tasks, has found significant utility in Drug Target Prediction (DTA) and Drug-Target Interaction (DTI) challenges [29, 31, 42, 43]. Recently, AiKPro introduced structurally validated multiple sequence alignments (svMSA) and multi-head attention (MHA) with cross attention between kinase and ligand and showed improved results compared to the previous models [22, 44]. Additionally, in KinScan, the integration of multi-scale context aggregation (MSCA) and deep context encoder (DCE) resulted in a significant improvement in the performance of bioactivity values [42]. Motivated by these advancements, our present study extends this approach with AiGPro. AiGPro is the single multi-task model based on a bi-directional multi-head cross-attention (BMCA) network with an applicability domain spanning the highest numbering, $n(n=231)$ of GPCRs. To our knowledge, no model exists with this number of human-druggable GPCRs within its applicability domain. Several

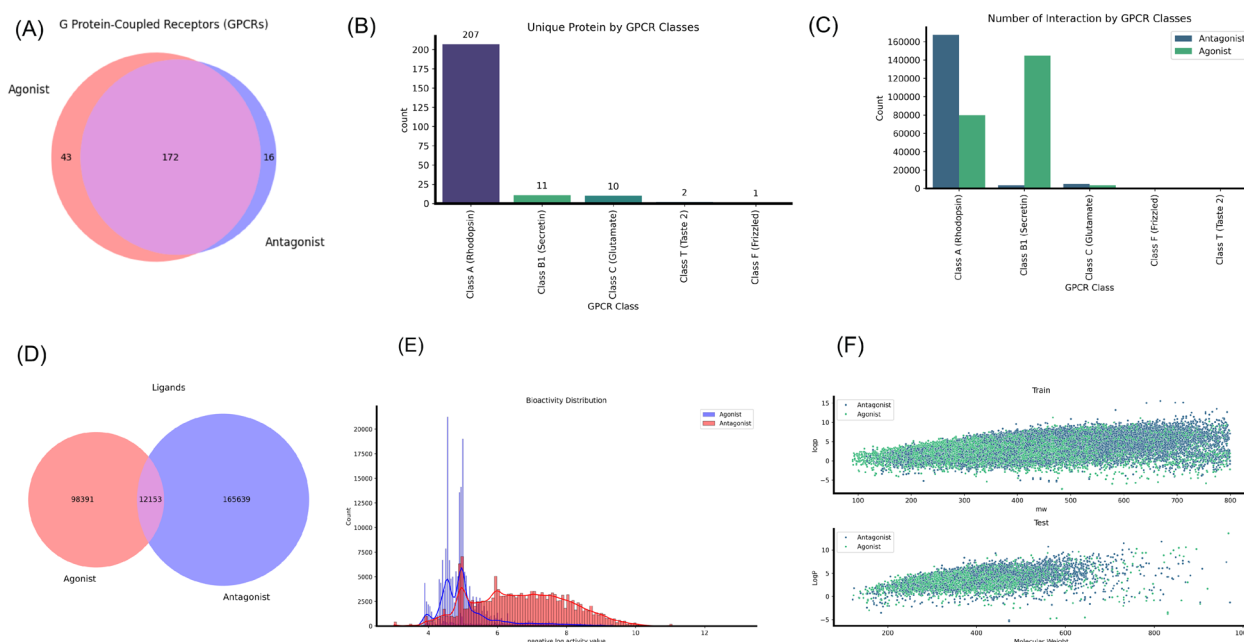


Fig. 1 The Details of Data Used in the Study. **A** displays the number of proteins with agonist, antagonist, or both data types. Similarly, **B** provides insights into the number of proteins each GPCR class classifies. **C** illustrates the total number of interaction pairs and their categorization into agonist, antagonist, and classes. **D** shows the count of unique ligands in different types of interaction with GPCRs. **E** displays the distribution of agonist and antagonist bioactivity. Finally, **F** demonstrates the relationship between the LogP and molecular weight of ligands for both the training and test datasets. Please note that (**A–E**) are specific to the training dataset

experiments demonstrated that it outperforms existing models in the accuracy and applicability domain, including ensemble models. Additionally, to enhance accessibility, we offer AiGPro as a web service, accessible free of charge at <https://aicadd.ssu.ac.kr/AiGPro>.

Methodology

Data collection and pre-processing

We focused on constructing a diverse and comprehensive dataset for model training to develop an effective model to address the current challenge. For these, we retrieved datasets from two databases: GLASS and GPCRdb. Last updated in February 2019, the GLASS database offered a repository of 562,871 curated GPCR-ligand interaction records featuring 342,539 ligands and 3,056 GPCRs with experimentally measured binding affinities. Simultaneously, the GPCRdb, updated as of October 25, 2023, contained data on 424 GPCRs, 217,578 ligands, and 481,718 bioactivities. Then we followed stringent filtration procedures, which excluded bioactivity values other than IC_{50} , K_i , and EC_{50} , duplicate pairs, non-sanitizable compounds by RDKit, and non-standard experimental kinetics values, keeping only the absolute values or those with “>” or “<” signs only. The resultant dataset featured 231 distinct human GPCRs and 276,183 small molecules, making 405,246 interactions comprising 44% antagonist and 56% agonist interactions. A dataset not in the above dataset containing 11,464 interactions with 11,259 unique ligands, of which 52.78% are unseen and with a similar agonist and antagonist ratio, was considered the

independent test set. More comprehensive details are in Fig. 1 for the training dataset. Additional file 1 is accessible at <https://aicadd.ssu.ac.kr/supportedgpcr>.

Distinguishing between antagonist and agonist datasets, we categorized the combined IC_{50} and K_i datasets as antagonistic, while the EC_{50} dataset represented agonists. Finally, in the remaining datasets, following [45], the experimental bioactivity (BA) values were transformed by adding some noise and then into the negative log of bioactivity (pBA) values as:

$$BA = BA \pm \text{random}(0, 0.3 \cdot BA),$$

$$+ \text{if } ' > ' \text{ in } BA, - \text{if } ' < ' \text{ in } BA, \text{ else } BA. \quad (1)$$

$$pBA = \alpha - \log(BA), BA \text{ in } \{IC_{50}, EC_{50}, K_i\} \quad (2)$$

where $\alpha = \{3, \text{if the value unit is in milimolar (mM)}$

$6, \text{if the value unit is in micromolar (uM)}$

$9, \text{if the value unit is in nanomolar (nM)}$

$12, \text{if the value unit is in picomolar (pM)}$

Sequence encodings

We used 1D sequences to represent both protein and chemical compounds. These 1D sequences consist of the MSA of proteins and Simplified Molecular Input

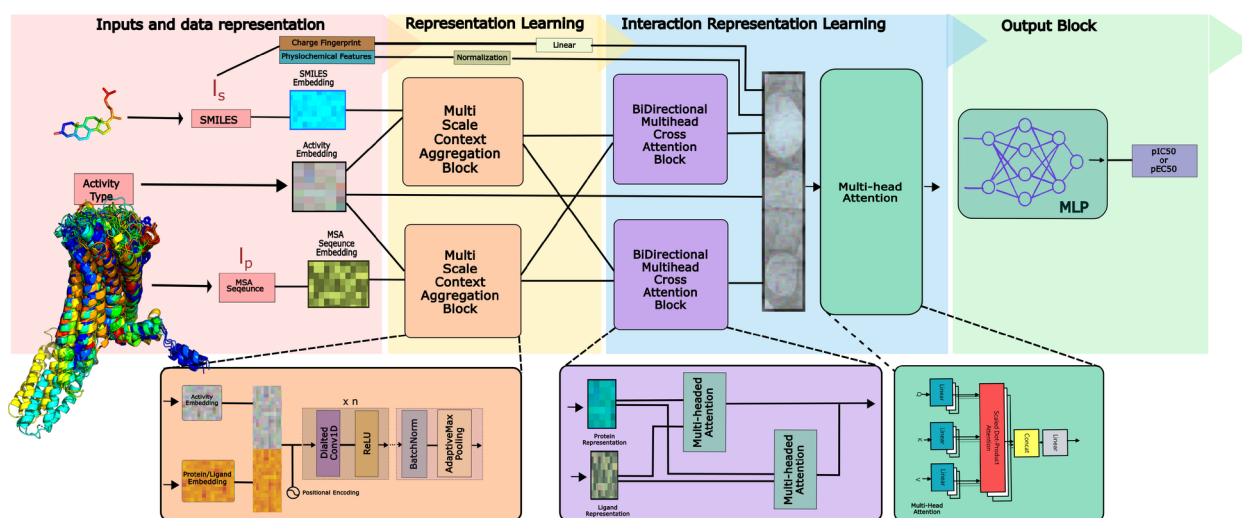


Fig. 2 Schematic Representation of the AiGPro Architecture. The diagram illustrates the proposed framework, which includes four modules: (1) Tokenizing and embedding the protein sequence from MSA and compound smiles inputs and data representation. (2) using the Multi-Scale Context-Aggregation module based on dilated convolution to extract multiscale features from both the input protein sequence and compound SMILES. (3) The bidirectional multi-head cross attention (BMCA) for intermolecular features between the protein and ligand (4) Output module to predict unknown interaction in a drug–target pair, which can address classification and regression tasks based on user consideration

Line Entry System (SMILES) strings of compounds. We employed structure-based alignment of protein sequences to encode the 3D structural information of proteins into a 1D sequence. This method provides a comprehensive representation of the structural features of proteins and allows us to gain valuable insights into their similarities and differences. On the other hand, SMILES is a concise ASCII string widely used for describing ligand chemical structures and efficiently encapsulating information about atoms, bonds, rings, and other molecular components.

Protein

For protein sequence, a structurally based MSA was performed using the complete GPCR protein sequence of all unique proteins, facilitated by the GPCRdb sequence alignment RESTful API available at <https://gpcrdb.org/services/>. We describe here the encoding of a single protein sequence from MSA of all GPCRs. Given the Protein MSA, $M = \{P_1, P_2, \dots, P_n\}$, where P_i is a single protein at the i -th index of MSA. So, $P_i = (a_1, a_2, \dots, a_n)$, $a \in [A, ' - ']$, where a_i represents the i -th amino acids, n represents the length of the sequence, 'A' represents the types of amino acids, and P_i is the i -th protein within MSA. In P_i , along with common amino acids, ' - ', it is also included due to the inherited feature of MSA, which represents gaps in the alignment. We encoded the protein sequence using a tokenized function, T , and obtained the tokenized sequence, $TP = \{t_1, t_2, \dots, t_n\}$, where each t_i is the token corresponding to a_i :

$$t = \{t_i | t_i \in T(a_i)\}, T : \Sigma \rightarrow [N]^t \quad (3)$$

where $[N]^t$ represent the set character of the token, which contains 25 elements, including $[TOKEN_{sp}]$, where $TOKEN_{sp} \in ["PAD", "UNK", "START", "STOP"]$. T enables encoding amino acids and gaps as discrete numerical values, facilitating computational operations and analysis within the MSA framework. In the study, $P_n = 231$ and $t_i = 1,900$, the maximum length of a protein sequence. The tokenized amino acid $t_i \forall i \in [N]^t$ is then embedded into d_p -dimensional vectors via an embedding layer.

Ligand

Consider a ligand, $C = \{c_1, c_2, \dots, c_m\}$, denotes the SMILES string of a ligand with m as the length of the string and c_i an i -th string within the SMILES. To get a tokenized smile, $TC = \{t_1, t_2, \dots, t_n\}$, where each t_i is the token corresponding to c_i :

$$t = \{t_i | t_i \in T(c_i)\}, T : \Sigma \rightarrow [D]^t \quad (4)$$

where t_n is the length of the smile string and $[D]^t$, represents the complete set of tokens for smiles, i.e., 575 characters vocabulary dictionary, which also includes $TOKEN_{sp}$. We then embedded the $t_i \forall i \in [D]^t$ to d_l -dimensional vectors via an embedding layer. We also utilized a positional embedding alongside a class token (agonist or antagonist), as shown in Fig. 2, that was embedded into dc with dimensions to d_l and d_p while using d_p and d_l of 32. Positional embedding was done in all sequences while class labels were concatenated to d_l and d_p .

Molecular feature encoding

Following [23], we calculated a 170-long vector molecular descriptors study to extract relevant features to evaluate the physicochemical attributes of chemical compounds using RDKit [46]. This descriptor includes Lipinski parameters for topological/topochemical descriptors of molecules, Atom-based LogP and molar refractivity (MR), Hybrid EState-VSA descriptors analogous to MOE van der Waals Surface Area (VSA) descriptors, QED descriptors, and Basic EState descriptors, etc. We also added the Gasteiger charge descriptor, a 512-dimensional vector that captures the charge distribution across all constituent atoms within the compound. Integrating these molecular features allows us to assess properties spanning diverse physicochemical domains of the molecules. This descriptor provides valuable insights into the compound's overall charge distribution, enhancing our understanding of its inherent characteristics.

AiGPro architecture

A schematic overview of the proposed multi-task model, AiGPro, is shown in Fig. 2. The model can be divided into the following parts: the input data representations, the multi-scale context aggregation (MSCA), the bi-directional multi-head cross-attention (BMCA), and the last output block for final prediction outputs. The MSCA block uses dilated convolution to expand its receptive convolution field without compromising the resolution or coverage to extract short and long-distance interaction information for the BMCA, which learns to extract meaningful interrelationships between distant atoms or residues. We used a similar setup for MSCA and Multi-head attention (MHA), as described in [23].

AiGPro builds upon the attention mechanism, scaled dot-product attention, introduced by Vaswani et al., and is a powerful method for calculating the connections and weighted sums between different elements in a given sequence [47]. MHA relies on self-attention, comprising multiple layers, followed by an FFN. In the architecture,

MHA layers are integral, each composed of multiple attention heads. These layers leverage scaled dot-product attention, requiring the utilization of query (Q), key (K), and value (V) matrices. These matrices, denoted as $W_i^Q \in \mathbb{R}^{d_{model} \times d_k}$, $W_i^K \in \mathbb{R}^{d_{model} \times d_k}$, $W_i^V \in \mathbb{R}^{d_{model} \times d_v}$ respectively, are learnable weight matrices. Here, $Q=K=V$ is the input protein and ligand representation for the MHA.

We employed the multi-head self-attention mechanism for n times, utilizing distinct linear projections to enhance performance. The MHA computes the self-attention operation in parallel on the projected iterations of queries, keys, and values, producing output values of d_{model}/h -dimensions. Where $W^T \in \mathbb{R}^{n d_v \times d_{model}}$ is a weighted parameter and $\frac{1}{\sqrt{d_k}}$ is scale factor. The output of MHA is further fed into the feed-forward layers, where R_{intra} is the learned representation.

$$Q_d = h_d W_d^Q, K_d = h_d W_d^K, V_d = h_d W_d^V \quad (5)$$

$$\begin{aligned} head &= \text{Attention}(Q_d, K_d, V_d) \\ &= \text{softmax}\left(\frac{Q_d K_d^T}{\sqrt{d_k}}\right) V_d \end{aligned} \quad (6)$$

$$MHA(h_d) = \text{concat}(head_1, \dots, head_n) W^T \quad (7)$$

$$R_{intra} = FFN\left(MHA(h_d) W_1^d + b_1^d\right) W_2^d + b_2^d \quad (8)$$

Bi-directional multi-head cross-attention module (BMCA)

Figure 2, shows the intra-molecular features and relationship between elements learned, and each DCE for protein and ligand output $(R_{intra}^p)^{d_{model}}$ and $(R_{intra}^l)^{d_{model}}$ for protein and ligand respectively. However, the information on the intermolecular dependency between the protein and ligand is still missing. Thus, within the BMCA, ligands and protein features undergo successive processing through the intermolecular bi-directional cross-attention layer, yielding multimodal data augmentation features specific to ligands and proteins and combined intermolecular features. BMCA is built upon MHA with h_{cross} attention heads, which take the learned representation $(R_{intra}^p)^{d_{model}}$ and $(R_{intra}^l)^{d_{model}}$ as the input.

In BMCA, for query protein, where $Q_{forward} = (R_{intra}^p)^{d_{model}}$ and $K_{forward} = V_{forward} = (R_{intra}^l)^{d_{model}}$ similarly for query ligand $Q_{backward} = (R_{intra}^l)^{d_{model}}$ and $K_{backward} = V_{backward} = (R_{intra}^p)^{d_{model}}$, the BMCA outputs

Table 1 Summary of the parameters used in developing the AiGPro

Parameters	AiG-ANT	AiG-AGO	AiGPro
Max length of SMILES	100	100	100
Max length of protein	1900	1900	1900
Protein embedding size	32	32	32
SMILES embedding size	32	32	32
Class embedding size	N/A	N/A	32
Batch size	512	512	512
Epoch	500	500	1000
Initial learning rate	0.001	0.001	0.003
Optimizer	AdamW	AdamW	AdamW
Dropout	0.1–0.5	0.1–0.5	0.1–0.5
Activation	Leaky-ReLU	Leaky-ReLU	Leaky-ReLU
Number of layers in MSCA	6/4	6/4	6/4
Number of layers in DCE	4	4	6
Number of layers in BMCA	2	2	2
Numbers of heads	16	16	16

N/A means Not Applicable

$R_{inter}^p \in \mathbb{R}^{a \times d_{model}}$ and $R_{inter}^l \in \mathbb{R}^{a \times d_{model}}$, is the learned representation of intermolecular feature. This feature is combined to form the final representation, as shown below.

$$R_{inter} = \text{Concat}\left(R_{inter}^p, R_{inter}^l\right) \quad (9)$$

Since BMCA is based on an attention mechanism, it has an $x(x=2)$ number of layers, followed by a residual connection and layer normalization. To counter overfitting, dropout layers are inserted post each computational layer, stochastically deactivating hidden unit activations to enhance model generalization beyond the training set.

The molecular features of the compounds are normalized and projected to a hidden state, MF , using an i -th projection layer, where $i \in [1, 2]$, h_i^c is the output vector of layer i , and $W_i^c \in \mathbb{R}^{d_{i-1} \times d_i}$ is learnable weighted parameter matrices, so the

$$h_i^c = FN(h_{i-1}^c + b_i^c) \quad (10)$$

The final context aggregation block merges the representations obtained from BMCA, backbone, and projected molecular features, as shown in Fig. 2. Additionally, we added the class embedding. This captures local and global information for inter and intra-molecular information, which helps refine the representation for downstream tasks. Then, it is passed through the final DCE to compressed combined global representation as,

$$R_{inter}^g = \text{Conc}(E^{class}, h_i^c) \quad (11)$$

which is then passed on to the final output block for final prediction.

Output block

The output block comprises a multi-layer perceptron (MLP), consisting of three fully connected neural network (FCN) layers. Each FCN layer, except the last one, to mitigate overfitting, utilizes a Leaky Rectified Linear Unit (Leaky-ReLU) activation function with a negative slope of 0.01, followed by a dropout layer. The output pBA , is the predicted bioactivity value between the protein and the ligand.

$$pBA = MLP(R_{inter}^g) \quad (12)$$

Model implementation and training detail

The model was developed and implemented using PyTorch and Python 3.11. It was trained on an NVIDIA 4090 24 GB with open-source CUDA 11.7 using the AdamW optimizer, with a learning rate of 0.003 and weight decay of 0.001. Dropout and L2 regularization techniques were applied to prevent overfitting. Overfitting was checked using validation data after every 10 epochs. Mixed precision and an early stopping strategy were utilized to optimize the training process. See Table 1 for more details.

Evaluation metrics

In the study, several evaluation metrics were computed to assess the model's performance on the test set and facilitate a comparison of its predictive power. We used Pearson's correlation coefficient (CC) for performance evaluation, Mean Square Error (MSE), and the correlation coefficient (R^2) to evaluate the performance of a model's predictions.

For model assessment, we computed the concordance Index (CI), which measures the concordance probability between the experimental and predicted values. CI can be defined as,

$$CI = \frac{1}{Z} \sum_{\delta_i > \delta_j} h(m_i - m_j) \quad (13)$$

where δ_i and m_i represent the experimental and predicted value for i -th data. With Z , the normalization constant, for the greater affinity δ_i and the smaller affinity δ_j , its prediction value is m_j and m_i respectively. $h(x)$ is defined as:

$$h(x) = \begin{cases} 1 & \text{if } x > 0 \\ 0.5 & \text{if } x = 0 \\ 0 & \text{if } x < 0 \end{cases} \quad (14)$$

The CI values range from 0 to 1, where 1 signifies the optimal outcome.

Furthermore, we utilized the Matthews Correlation Coefficient (MCC), a robust statistical metric perfect for evaluating models on binary classification [48]. In addition to MCC, we also employed the Area Under the Receiver Operating Characteristic curve (AUC-ROC) and Cohen's kappa to comprehensively evaluate the performance of our models in classification tasks. To ensure a thorough assessment, we conducted a stratified K-fold CV ($K=10$) to confirm the usability, reliability, and generalizability of AiGPro.

Web server implementations and deployment

To provide an accessible end-to-end solution, we have deployed AiGPro as a web platform using FastAPI and Nginx as the backend and reverse proxy server for load balancing. This reduces the difficulty for users without a computational background to test the model without downloading and installing anything. The User Interface (UI) is developed using React JSX, Vite, and Tailwind CSS frameworks. The predicted target activity value table is presented using React DataTables, while interactive plots and figures are generated using Plotly.js and the D3 library.

Real-world application test: a case study on Alzheimer's disease (AD)

As proof of concept and to test the applicability domain, we tested our models and their limitations in real-world applications. Our focus was on addressing the problem of AD, so we curated GPCR data involved in the disease, not in the training dataset, to use as an external test dataset. This dataset consists of 4895 unique ligands, which form 6050 GPCR-ligand pairs, of which 5508 are antagonist interactions and 542 are agonist bioactivity data. The dataset contains 8803 unique ligands interacting with four GPCRs. These receptors are Adenosine receptor A2a (P29274), Muscarinic acetylcholine receptor M1 (P11229), Muscarinic acetylcholine receptor M3 (P20309), and Muscarinic acetylcholine receptor M2 (P08172). It is known that these proteins have a role to play in AD. These proteins are dysregulated in the cognitive area of AD patients [33, 34]. Some of these GPCRs have garnered significant interest due to numerous studies supporting them as credible targets for repurposing existing drugs or designing and discovering new drugs with clinical potential [49].

The adenosine receptor A2a interacts with 2,662 unique ligands to form 2,695 interactions. The Muscarinic acetylcholine receptor M1 interacts with 1,265 unique ligands to create a total interaction of 1,284. The

Muscarinic acetylcholine receptor M3 interacts with 1,078 unique ligands to form 1,084 interaction data. The Muscarinic acetylcholine receptor M2 interacts with 982 ligands to form 987 interaction data. See Table 5 for more details on the AD test dataset.

Results and discussion

Model development

To develop robust prediction models for orphan GPCRs, we curated a comprehensive dataset consisting of 98,391 agonistic ligands, 165,639 antagonistic ligands, and 12,153 dual agonist-antagonistic ligands, covering 231 GPCRs as shown in Fig. 1. Of these GPCRs, 43 had only agonistic ligand interactions, 16 proteins had exclusively antagonistic ligand activities, and 172 GPCRs with at least one ligand exhibited both agonistic and antagonistic activities. This dataset was extracted from multiple publicly available databases. GPCRs are complex because they can adopt different conformational states, resulting in a single ligand exhibiting different activities (e.g., agonist, antagonist, or both). Consequently, traditional single-task or multi-task models, which predict only bioactivity value, are insufficient for distinguishing between these states, making them unsuitable for profiling applications.

In our earlier work, AiKPro [22], we utilized one-hot encoding with svMSA for protein representation and 3D ensemble features for ligands, successfully capturing their structural information for bioactivity prediction in kinases. While this approach yielded accurate results, the requirement for computationally expensive 3D ensemble features for ligands was a limitation. Subsequently, in KinScan [23], we advanced this methodology by employing embedding-based representations with MSCA and DCE. This innovative approach combined dilated convolutions with data-specific feature engineering for svMSA. By doing so, we eliminated the need for 3D ensemble ligand features while achieving superior predictive performance to our and existing models for Kinases.

For the current work on GPCRs, we adopted a similar foundational approach from KinScan while addressing their inherent complexities. GPCRs are membrane proteins with multi-state interactions, which cause them to exhibit different bioactivities for the same ligand under varying conditions.

To tackle this, we developed BMCA, a novel methodology that captures structural information tailored to the required output. BMCA enables our model to predict bioactivity values for both agonist and antagonist dynamically. For instance, if the input specifies agonistic activity, the model predicts a value distinct from that of

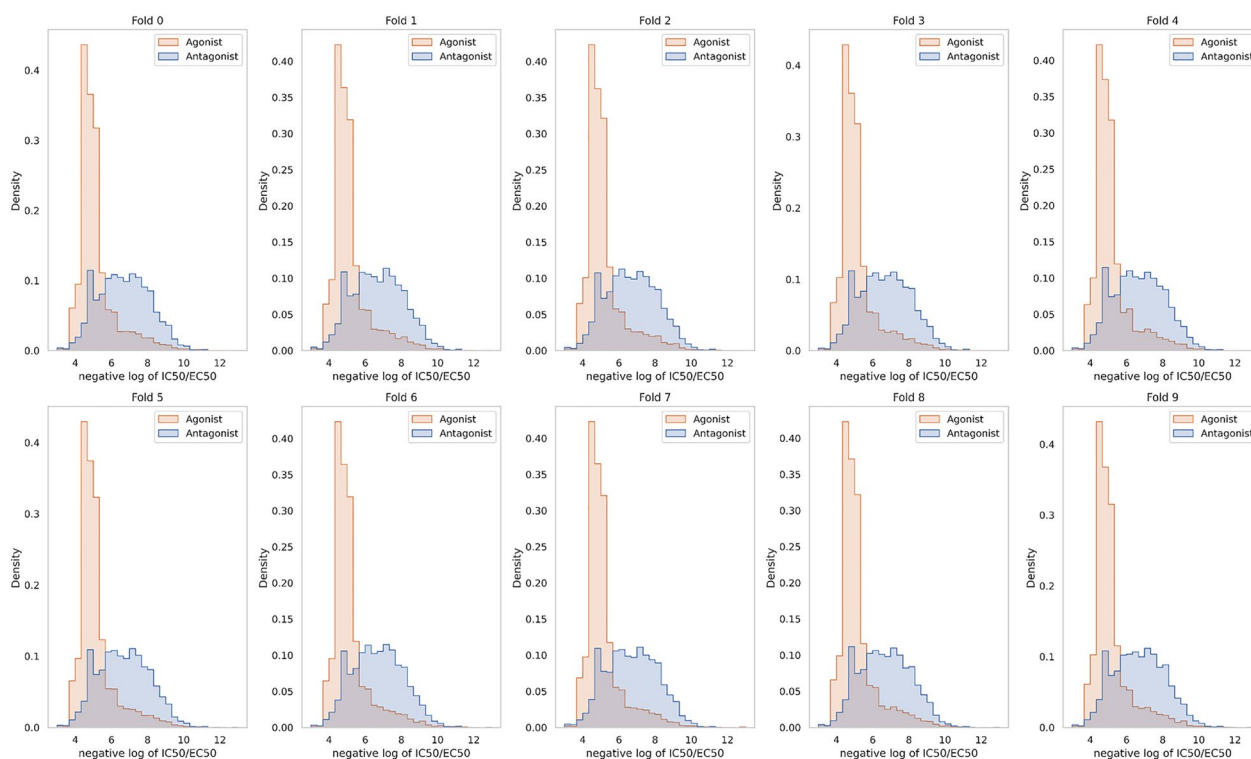


Fig. 3 Distribution of End Points for each fold in Cross-validation

antagonistic activity, even for the same ligand. This state-dependent prediction capability makes BMCA highly suited for modeling the complex, multi-state interactions characteristic of GPCRs.

Performance evaluation

Accurately predicting the binding affinity between proteins and compounds is crucial in drug discovery to differentiate between meaningful interactions and those with secondary targets, also known as off-targets. GPCRs are one of the most important targets, and many drugs target them. However, existing models only cover a single target or a small number of GPCRs because the complexity of GPCRs, being membrane proteins, limits the availability of high-quality data. To overcome this issue, an effort has been made to combine multiple ML models, creating an ensemble model to predict GPCR bioactivity values [40, 41]. Even though this approach adds integration and computation complexity, limitations remain in generality, accuracy, and applicability to broad GPCRs for large-scale profiling.

In this regard, we initially developed two separate models, AiG-ANT and AiG-AGO, to predict the bioactivity of antagonists and agonists against GPCRs. We trained these models on separate datasets comprising 183,466 antagonist and 229,312 agonist instances and evaluated them using distinct test sets for antagonist and agonist samples, respectively. In this study, we extensively evaluated the model on test data to ensure its reliability in real-world scenarios and demonstrate its strong generalization ability to predict unseen compounds. As shown in Table 3, the AiG-ANT model performed well on the independent antagonist test set, with R^2 value of 0.773 and a corresponding CC of 0.879 for antagonist bioactivity predictions. The AiG-AGO model also showed promising results, with R^2 of 0.719 and a CC of 0.853 for agonist bioactivity predictions on the independent agonist dataset.

However, a discrepancy in performance between agonist and antagonist evaluations was evident. This was due to the limited range of EC_{50} values for agonists. Around 90% of all agonist instances had pEC_{50} values between 4 and 5. In contrast, antagonist data had a more uniformly normally distributed, with a standard deviation of about 1.39, compared to the narrower range of 1.04 for agonist datasets. To address this issue, we developed a multi-task model, AiGPro, and trained it on a combined agonist and antagonist samples dataset. AiGPro showed superior performance to the single-task models, with a R^2 of 0.829 and a CC of 0.912, surpassing the individual single-task models. This approach improved performance significantly by over 7–16% and allowed us to integrate

bioactivity categories seamlessly. A similar trend of increased performance on combined datasets than single ones was also observed in previous research [41]. This can be attributed to the enhanced ability of DL models to exploit larger volumes of data and the use of conditional labeling to facilitate better fitting to data distributions.

Furthermore, to mitigate concerns regarding overfitting, our study conducted a rigorous tenfold stratified CV, as shown in Fig. 3 analysis, and evaluated performance on an independent test set, yielding similar results as shown in Table 3. Thus, our framework presents a versatile, general, and innovative approach to exploring the intricate mechanisms underlying agonistic and antagonistic ligand interactions in GPCR systems. The optimal settings used to train AiGPro depend on various parameters, such as embedding size, the number of heads in MHA, the number of layers in MSCA and BMCA, the number of epochs, the dropout rate, the learning rate, and so on. These parameters are crucial for determining the performance of AiGPro and were determined based on KinScan and some hyperparameter searches. For more detailed specifications of these parameter settings, see Table 1 and Additional File 2.

Comparison with existing options

Based on our knowledge, AiGPro is the first multi-task neural network based on the transformer's attention mechanism architecture approach that can accurately predict the bioactivity values, i.e., antagonist IC_{50} and agonist EC_{50} of small molecules to profile against 231 GPCRs. We found that pdCSM-GPCR, a graph-based model, is similar to our model's applicability; however, this model is limited to only 36 GPCRs, significantly limiting its applicability domain.

We compared the performance of AiGPro against pdCSM-GPCR to predict ligand activity using a dataset retrieved from pdCSM-GPCR's test dataset. AiGPro's capability to predict both agonist and antagonist activity values, as shown in Table 3, is a crucial consideration for successful therapeutic development efforts, especially in GPCR-related drug discovery. However, the significant limitation of existing models, including pdCSM-GPCR, is its inability to distinguish such crucial information. Since this test dataset doesn't contain an activity type label, we considered it an outlier dataset for AiGPro, which is a significant challenge in accurately predicting activity values. We included both activity types and considered only the lowest value in the metric against the pdCSM-GPCR.

The result, summarized in Table 2 and Additional file 4 Figure S1 and Figure S2, shows that AiGPro performed well against pdCSM-GPCR for large numbers of GPCRs, with MSE ranging from as low as 0.01 for Q99835 to 2.2. However, we observed that AiGPro performed

Table 2 Comprehensive Performance Metrics of pdCSM-GPCR and AiGPro Models for 36 GPCRs supported by pdCSM-GPCR, including Pearson and Spearman and Mean Squared Error (MSE)

Metric	Pearson			MSE			Spearman		
	UniProt ID	AiGPro Agonist	AiGPro Antagonist	pdCSM-GPCR	AiGPro Agonist	AiGPro Antagonist	pdCSM-GPCR	AiGPro Agonist	AiGPro Antagonist
P08173	0.677697	0.844019	0.927161	0.598459	0.262448	0.138784	0.681418	0.811225	0.920255
P08908	0.689659	0.921445	0.913819	1.440755	0.197048	0.244769	0.725641	0.930697	0.915411
P08912	0.558878	0.73516	0.96047	0.389232	0.23069	0.039637	0.643617	0.795608	0.931363
P0DMS8	0.724056	0.898625	0.837471	1.079031	0.309748	0.416983	0.71744	0.902301	0.929995
P20309	0.756877	0.857717	-0.18575	2.387652	0.741582	16.83852	0.752055	0.830525	0.239374
P21452	0.903191	0.977033	0.661544	0.632052	0.106288	1.393349	0.890782	0.970373	0.868128
P21917	0.763711	0.890759	0.894257	0.439251	0.198539	0.219516	0.792558	0.883109	0.891361
P24530	0.790824	0.858437	0.926488	0.5765	0.340872	0.28856	0.845828	0.925262	0.923018
P28335	0.783483	0.925001	0.936922	0.525033	0.148203	0.165385	0.778624	0.92579	0.937908
P29275	0.57747	0.747991	0.89956	1.744522	0.576609	0.22598	0.604479	0.782773	0.894269
P30542	0.63934	0.90017	0.396229	1.493945	0.250213	1.440032	0.551049	0.930075	0.876307
P30968	0.577188	0.492209	0.339559	2.246996	2.080604	2.551277	0.469937	0.363065	0.799985
P34995	0.780087	0.860241	0.577697	0.64427	0.328886	0.924773	0.83424	0.911129	0.534206
P35346	0.44117	0.479922	0.65292	1.939671	2.200727	0.843807	0.333241	0.423323	0.650743
P35348	0.899096	0.962053	-0.15992	0.390727	0.120603	8.235974	0.911268	0.96074	0.526311
P35372	0.732431	0.846547	0.381958	1.671303	0.620345	3.148592	0.722602	0.837374	0.802032
P41180	0.814046	0.948219	0.84282	0.595652	0.096359	0.245888	0.797648	0.939531	0.814971
P46663	0.882107	0.935077	0.752952	0.704371	0.301326	1.084366	0.872538	0.936141	0.833231
P47871	0.7521	0.883138	0.851745	0.994021	0.253084	0.471346	0.688865	0.809073	0.800408
P47900	0.632413	0.757002	0.93903	1.304861	0.439505	0.149359	0.675703	0.900808	0.900456
P48039	0.78483	0.933192	-0.32359	1.172908	0.235479	9.592626	0.794298	0.935882	0.406757
P50406	0.813097	0.923785	0.941495	0.735113	0.222674	0.202607	0.84594	0.943349	0.940951
P51677	0.916871	0.969147	0.524032	0.319415	0.089995	1.309028	0.929045	0.976074	0.879858
Q14416	0.904959	0.944118	0.939619	0.210774	0.096948	0.086333	0.905397	0.941748	0.89801
Q14833	0.390707	0.312899	-0.54542	2.303484	2.421646	6.00078	0.805074	0.715054	0.660051
Q16602	0.451143	0.536767	-0.06658	2.691533	2.156264	9.260116	0.425713	0.525492	0.481879
Q8TDS4	0.858214	0.907132	0.771218	0.319798	0.149885	0.350926	0.866247	0.903202	0.754774
Q8TDU6	0.981837	0.874889	0.880415	0.072351	0.563678	0.419429	0.979498	0.872989	0.87819
Q96LB2	0.807737	0.880264	0.819568	0.252343	0.210351	0.233144	0.873239	0.890536	0.745612
Q99500	0.896725	0.911844	0.531145	0.174193	0.129037	0.602572	0.91287	0.928918	0.467122
Q99705	0.826176	0.944241	0.883057	0.606932	0.097271	0.224144	0.827514	0.941554	0.887913
Q99835	0.70499	0.990305	0.889806	0.880702	0.015348	0.164317	0.73248	0.987365	0.917692
Q9H228	0.82701	0.838706	0.737199	0.415411	0.738059	0.620671	0.713968	0.765747	0.82804
Q9HC97	0.851701	0.778585	0.911147	0.413254	0.862635	0.28222	0.766518	0.665466	0.917893
Q9Y5N1	0.866684	0.95228	0.873469	0.376423	0.142348	0.340459	0.868995	0.942514	0.852287
Q9Y5Y4	0.8684	0.969928	0.734544	0.564619	0.088746	0.606321	0.869558	0.974374	0.748595

relatively worse in some GPCRs, like Q14833, P30968, and Q14833, with MSE as high as 2, even though this MSE is lower than pdCSM-GPCR in some cases.

Further analysis was conducted on proteins, as presented in Table S1; we observed that the imbalance in the dataset ratio between agonists and antagonists likely contributed to the higher MSE values for two of the proteins. Interestingly, despite having a balanced dataset, the

protein associated with UniProt ID Q9HC97 also exhibited poor performance. A deeper investigation revealed that most data for Q9HC97 consisted of log activity values lower than 5, suggesting that a large proportion of inactive data can negatively impact the model's predictive accuracy.

This study highlights the unique strengths and limitations of AiGPro and pdCSM-GPCR in predicting

Table 3 Comparison of performance metrics, such as MSE, MAE, and CC, for AiGPro, compared to similar existing models. Bold text indicates the best result

MODEL	TARGET	MSE ↓	MAE ↓	CC ↑
STL-AG	EC ₅₀	0.96	0.46	0.83
MTL-AG	EC ₅₀	0.29	0.37	0.80
STL-ATG	EC ₅₀	0.50	0.47	0.83
MTL-ATG	EC ₅₀	0.27	0.35	0.83
MTL-AG-ATG	EC ₅₀	0.24	0.30	0.85
MTL-AG-ATG-FS	EC ₅₀	0.24	0.30	0.85
MTL-AG-ATG-M2V	EC ₅₀	0.27	0.33	0.85
MTL-AG-ATG-M2V-FS	EC ₅₀	0.27	0.33	0.84
Chemprop (Multi)	EC ₅₀ & IC ₅₀	0.57	0.54	0.86
AiGPro	EC ₅₀ & IC ₅₀	0.35	0.38	0.91
AiGPro (CV)	EC ₅₀ & IC ₅₀	0.363 (0.004)	0.409 (0.004)	0.907 (0.001)

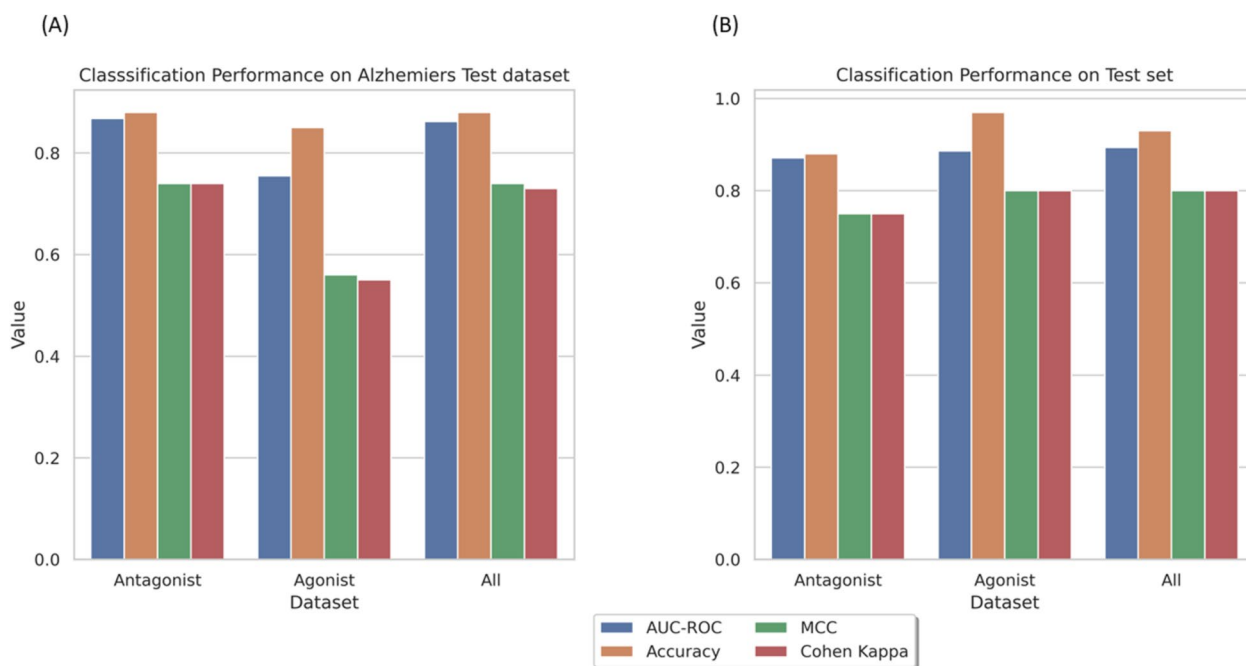
* The values inside parentheses indicate the Standard Deviation, and CV represents Cross-Validation

ligand activity for class A GPCRs. While pdCSM-GPCR shows some strengths in specialized scenarios, AiGPro's broader applicability and generalizability across a more comprehensive range of GPCRs make it a promising tool for advancing GPCR-targeted drug discovery. However, the study also underscores the need for models that can

accurately distinguish between different types of ligand activities, an area that remains critical for the field.

Wei-Cheng et al. recently published models that were trained on a dataset of 200 GPCRs using EC₅₀ data to predict agonist and antagonist activity values with single-task (STL-AG) and multitask (MTL) models [41]. However, there are concerns about potential biases resulting from merging training and validation datasets, particularly in the MTL training of models. This is an essential difference from the methodology used by AiGPro, which does not incorporate such merging, resulting in a more robust and impartial evaluation framework.

As shown in Tables 2 and 3, our single-task models, the AiG-ANT and AiG-AGO, have demonstrated exceptional predictive performance with CC values of up to 0.879 for antagonists and 0.853 for agonists. In contrast, the best-performing models among the STL and MTL models, and also integrating the training and validation data within the multitask framework (MTL-AG-ATG), along with various feature combinations including additional mol2Vec (M2V) feature vectors, results in slight improvements with CC values reaching up to 0.85 from 0.80, which is lower than most of AiG models, except the AiG-AGO-B and AiG-ANT-B. However, AiGPro stands out as the best performer, exceeding these ensemble models with a remarkable CC of 0.913 and R² of 0.833 predictions on the test set. These suggest that our novel multi-task attention-based bidirectional model can learn complex relationships between GPCRs and ligands. The

**Fig. 4** Performance of AiGPro on classification task on Test dataset and Alzheimer's Disease data

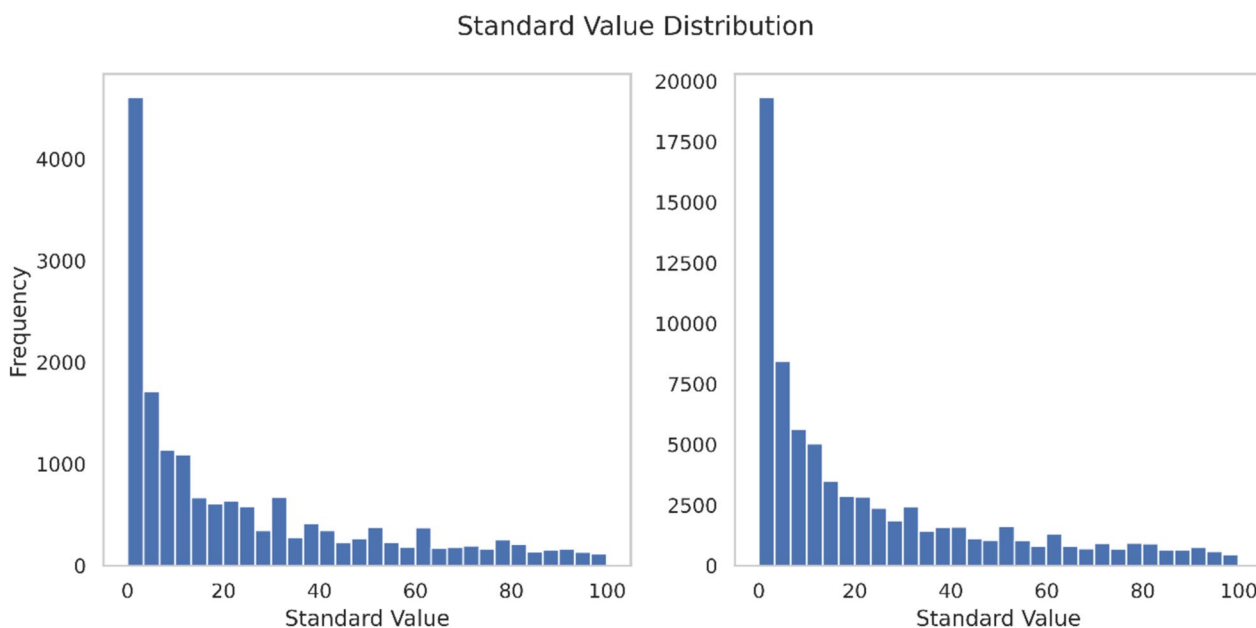


Fig. 5 Count of Active interaction for agonist and antagonist

Table 4 Ablation study on the effect of BMCA on single and multi-task Models

MODEL	BMCA	$R^2 \uparrow$	CC \uparrow	CI \uparrow
AiG-AGO	×	0.719	0.853	0.833
AiG-ANT	×	0.773	0.879	0.827
AiG-AGO-B	O	0.613	0.794	0.809
AiG-ANT-B	O	0.670	0.828	0.730
AiGPro	×	0.551	0.759	0.764
AiGPro	O	0.829	0.912	0.848

Please note that in the model development, 'O' represents the used features, while '×' represents the unused features. BMCA=Bi-directional Multi Head Cross Attention module. Bold text indicates the best result

disparities in MSE and MAE across models in Table 3 underscore the inherent scale dependency of these metrics, necessitating careful consideration during comparative analyses.

Furthermore, we evaluated the model's efficacy in identifying active and inactive ligands, defining active ligands as those with a potency of less than 100 μM . As depicted in Fig. 4A, B, AiGPro exhibited overall robust performance, with a slight decrease in performance for agonists compared to antagonists. This discrepancy may be attributed to the relatively smaller number of active ligands in the training dataset, see Fig. 5, influencing the model's ability to generalize effectively to this category.

Overall, this demonstrates that the AiGPro has a balanced capability for generalization and accuracy in

predicting with a broad applicability domain, enabling large-scale high throughput screening for GPCR ligands.

Ablation study

In this study, we aimed to evaluate the importance and efficiency of different components of the AiGPro design for extracting meaningful information that can help make accurate bioactivity predictions. To achieve this, we use the same datasets for training and testing and conduct ablation experiments to understand the contribution of each component, such as MSCA, DCE, molecular features, and BMCA. Although the importance of some of these components has been highlighted in previous studies [23], BMCA is a new addition that requires a dedicated examination of its efficacy and relevance. Thus, we conducted ablation experiments to assess the impact of the BMCA module on the AiGPro model's performance.

As shown in Table 4, the removal of BMCA had a substantially varied influence on the predictive capabilities of the single and multi-task models. The single-task models without BMCA, namely the AiG-AGO and AiG-ANT, performed very well; however, on adding BMCA to this model (AiG-ANT-B and AiG-AGO-B), a significant reduction in performance was observed, with CC dropping to as lowest of 0.829 and 0.794 from 0.879 and 0.853 for ANT and AGO models respectively. These models were based on a previous study, which was well designed for predicting bioactivity, also held in the current study. Nevertheless, the absence of the BMCA in the multi-task model resulted in a significant decrease in performance,

Table 5 Overview of data in detail for external GPCR application test related to Alzheimer's disease

UniProt	Protein name	Unique ligands	Interactions	Antagonist	Agonist
P29274	Adenosine receptor A2a	2656	2695	2556	139
P11229	Muscarinic acetylcholine receptor M1	1213	1284	1020	264
P08172	Muscarinic acetylcholine receptor M2	941	987	914	73
P20309	Muscarinic acetylcholine receptor M3	1027	1084	1018	66
All	–	4895	6050	5508	542

Table 6 Comparative analysis of AiGPro with other available methods on the Alzheimer's data

UniProt	Methods	All R^2	Ago R2	Anta R2	All CI	Ago CI	Anta CI	All MSE	Ago MSE	Anta MSE	All CC	Ago CC	Anta CC
P29274	AiGPro	0.688	0.458	0.701	0.830	0.785	0.831	0.515	0.999	0.489	0.830	0.687	0.838
	pdCSM-GPCR	NS	NC	NC	NS	NC	NC	NS	NC	NC	NS	NC	NC
	Chemprop(Ago)	-1.229	0.298	-1.331	0.526	0.769	0.520	3.694	1.292	3.842	0.076	0.607	0.052
	Chemprop(Anta)	0.719	-0.391	0.786	0.830	0.563	0.850	0.465	2.562	0.350	0.850	0.186	0.888
	Chemprop(Multi)	0.724	-0.291	0.785	0.832	0.556	0.852	0.456	2.378	0.351	0.852	0.136	0.889
P11229	AiGPro	0.712	0.279	0.789	0.829	0.722	0.856	0.564	1.035	0.442	0.844	0.573	0.889
	pdCSM-GPCR	NS	NC	NC	NS	NC	NC	NS	NC	NC	NS	NC	NC
	Chemprop(Ago)	-0.475	0.626	-0.672	0.568	0.815	0.525	2.896	0.535	3.507	0.199	0.808	0.073
	Chemprop(Anta)	0.630	-0.526	0.834	0.798	0.508	0.872	0.726	2.191	0.346	0.804	0.106	0.917
	Chemprop(Multi)	0.653	-0.371	0.835	0.802	0.525	0.871	0.679	0.968	0.345	0.812	0.153	0.915
P08172	AiGPro	0.805	0.587	0.810	0.869	0.811	0.870	0.465	0.715	0.446	0.899	0.772	0.902
	pdCSM-GPCR	NS	NC	NC	NC	NC	NC	NS	NC	NC	NS	NC	NC
	Chemprop(Ago)	-0.861	0.849	-1.05	0.520	0.870	0.498	4.455	0.259	4.790	0.045	0.940	-0.016
	Chemprop(Anta)	0.790	-0.344	0.848	0.863	0.612	0.883	0.500	2.323	0.354	0.897	0.271	0.926
	Chemprop(Multi)	0.813	-0.127	0.859	0.868	0.660	0.886	0.447	1.948	0.327	0.905	0.393	0.929
P20309	AiGPro	0.865	0.491	0.862	0.895	0.732	0.893	0.417	0.570	0.408	0.930	0.754	0.929
	pdCSM-GPCR	-0.703	NC	NC	0.778	NC	NC	3.898	NC	NC	0.279	NC	NC
	Chemprop(Ago)	-0.702	0.781	-0.885	0.552	0.820	0.531	5.277	0.245	5.604	0.201	0.901	0.156
	Chemprop(Anta)	0.863	-1.025	0.897	0.895	0.558	0.905	0.424	2.272	0.304	0.929	0.244	0.947
	Chemprop(Multi)	0.858	-0.892	0.889	0.893	0.531	0.903	0.438	2.122	0.329	0.927	0.228	0.944
All	AiGPro	0.765	0.472	0.784	0.854	0.779	0.859	0.500	0.925	0.458	0.875	0.693	0.886
	pdCSM-GPCR	NA	NC	NC	NA	NC	NC	NA	NC	NC	NA	NC	NC
	Chemprop(Ago)	-0.846	-1.00	0.625	0.536	0.519	0.824	3.933	4.255	0.657	0.124	0.075	0.794
	Chemprop(Anta)	0.756	-0.318	0.839	0.845	0.575	0.873	0.519	2.314	0.342	0.873	0.236	0.917
	Chemprop(Multi)	0.766	-0.191	0.838	0.847	0.592	0.872	0.499	2.089	0.342	0.875	0.272	0.916

'Anta' means Antagonist, 'Ago' means Agonist, 'Multi' means Multi-Task, 'NC' means Not Capable to distinguish between agonistic or antagonistic ligand activity, 'NS' means Not Supported and 'NA' means Not applicable

with a CC of only 0.759, approximately 5% lower than the weakest single-task model, namely the AiG-AGO-B. However, including the BMCA led to a substantial improvement in performance, surpassing even the strongest single-task models and achieving a CC of 0.912.

As a result, the single-task model cannot take advantage of BMCA, and these models perform inferiorly with the proposed architecture. Overall, our ablation experiments provide compelling evidence supporting the significance of the BMCA module within the AiGPro

architecture. By elucidating its critical role in information extraction and predictive accuracy, our study contributes valuable insights into advancing computational methodologies for bioactivity prediction in drug discovery and development using a multi-task model.

Applicability test on Alzheimer's related proteins

To verify the practical applicability of the model, we conducted a case study on GPCRs implicated in AD, namely Adenosine receptor A2a, Muscarinic acetylcholine

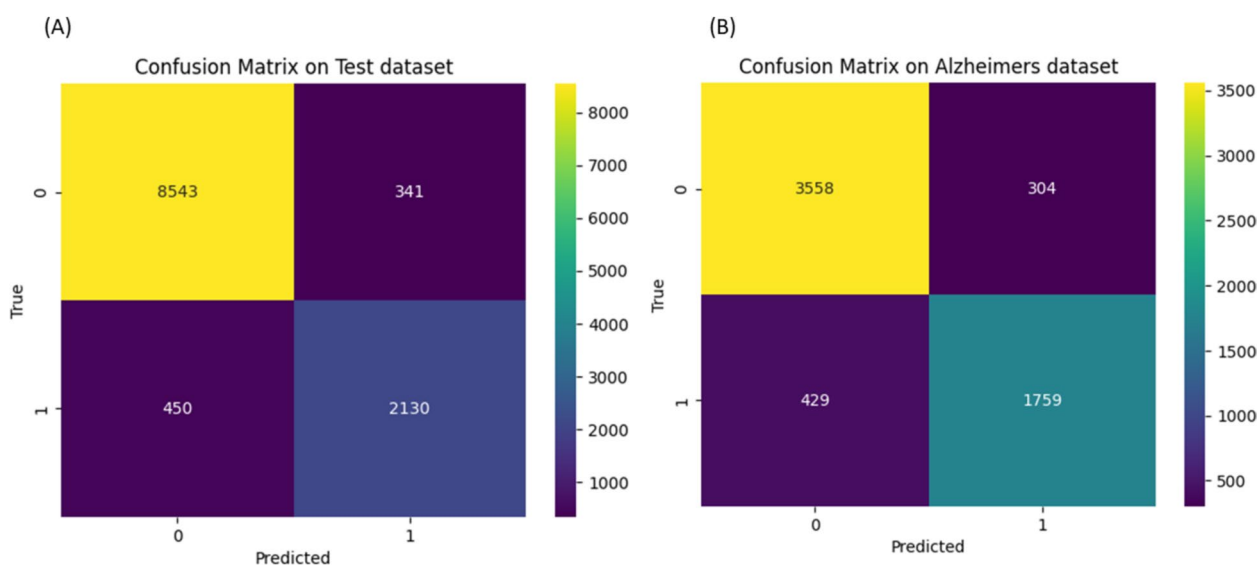


Fig. 6 Confusion Matrix of AiGPro on Classification task on Alzheimer's Disease and Test Dataset

receptor (mAChR) M1, mAChR M2, and mAChR M3. The A_{2A} adenosine receptor, a vital member of the P1 purinergic receptor family, significantly influences the pathophysiology of various neurodegenerative disorders, including AD. Its regulatory effects on neurons and glial cells modulate synaptic transmission and neuroinflammation. Notably, the A_{2A} receptor is the most extensively studied adenosine subtype concerning its effects on neurodegenerative diseases and the availability of selective receptor antagonists currently undergoing clinical evaluation.

Likewise, the involvement of mAChR M1, M2, and M3 in AD is well-documented, with several ongoing clinical investigations [49]. Notably, the M1 subtype has witnessed the development of orthosteric ligands like xanomeline and, recently, HTL9936, progressing from preclinical models to human trials. While allosteric ligands for M1-mAChR are in early developmental stages, promising data from preclinical studies underscore their potential efficacy [49].

Experimental evidence underscores the crucial role of M1-mAChR in cognitive function, supported by studies demonstrating cognitive deficits upon genetic ablation or pharmacological inhibition of M1-mAChR signaling in rodents. Conversely, activation of M1-mAChR has been shown to ameliorate learning and memory deficits in preclinical models of neurodegeneration and human patients with central nervous system disorders such as schizophrenia [49–51].

The M2-mAChR subtype exhibits widespread expression throughout crucial brain regions involved in cognition, and its antagonism has shown potential in rescuing

cognitive deficits in neurodegeneration in rodent models [52]. In contrast, the M3-mAChR subtype exhibits the lowest expression levels in the central nervous system, primarily localized in the hypothalamus. While its precise role remains unclear, studies using knockout and phospho-deficient knockin mice suggest a potential involvement of M3-mAChR in cognitive function [53].

We evaluated the predictive capabilities of AiGPro in comparison to existing models, such as pdCSM-GPCR, and general methodologies like Directed Message Passing Neural Network (D-MPNN) models implemented in Chemprop [54]. For Chemprop/D-MPNN, we trained multiple models: two single-task models (one for agonists and another for antagonists) and a multi-task model for both activities, using the same dataset. These models were then tested on the Alzheimer's dataset, as shown in Table 5, which included ligands with both agonistic and antagonistic activities, providing challenges to the models like pdCSM, which do not differentiate between these activities. Notably, only one of the four GPCRs analyzed falls within pdCSM-GPCR's scope.

As shown in Table 6, Figure S3, and Figure S4, AiGPro outperformed other predictive models across various metrics. However, there were instances where Chemprop models delivered comparable or slightly superior performance. For protein P20309, AiGPro achieved the highest R^2 of 0.865 and the lowest MSE of 0.417 for all ligands. Chemprop(Multi) and Chemprop(Anta) exhibited R^2 values close to AiGPro's, at 0.858 and 0.863, respectively. However, their MSE values were slightly higher, reflecting less precise predictions. Similarly, for P08172, Chemprop(Anta) and Chemprop(Multi) achieved

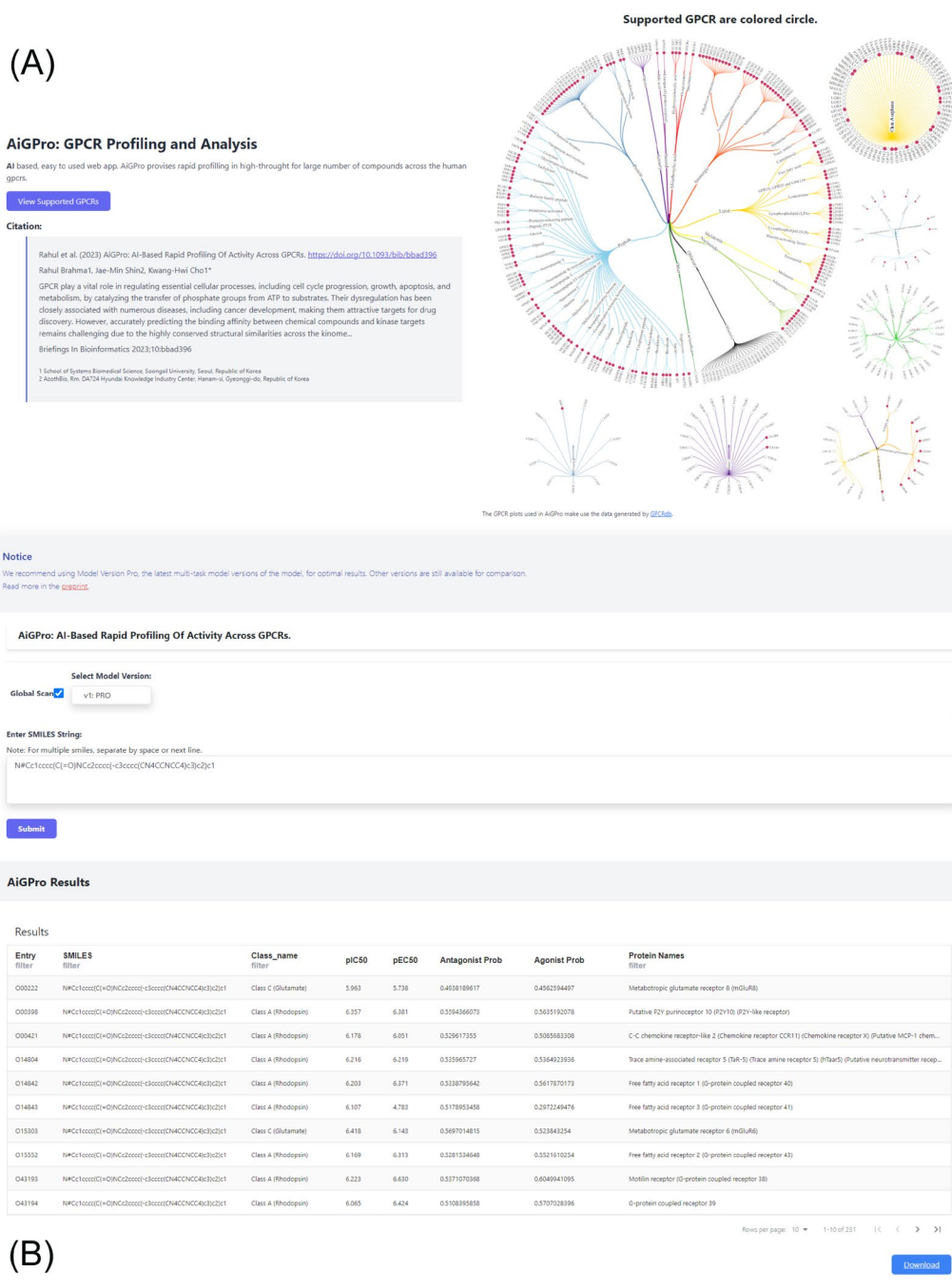


Fig. 7 An overview of the AiGPro end-to-end web platform with a user-friendly interface for using the AiGPro model easily. **A** The main page of the AiGPro web server shows inputs for smile queries. **B** The resultant output, which includes Antagonist and Antagonist values from AiGPro prediction, can be downloaded for further analysis

comparable or marginally better R^2 values of 0.790 and 0.813, respectively, compared to AiGPro's 0.805. Additionally, their MSE values for all ligands were close to AiGPro's 0.465, with Chemprop(Multi) slightly outperforming AiGPro. For P29274, Chemprop(Anta) and

Chemprop(Multi) performed marginally better than AiGPro in R^2 and MSE. In contrast, AiGPro outperformed all other models for P11229, achieving an R^2 of 0.712 compared to Chemprop(Anta) and Chemprop(Multi), which scored 0.630 and 0.653, respectively.

One of the most notable trends is observed in Chemprop's performance for agonist and antagonist predictions. While Chemprop models, particularly Chemprop(Multi) and Chemprop(Anta), demonstrated competitive performance for antagonist activity prediction, all Chemprop models failed for agonistic activity prediction. Negative R^2 values, such as -1.229 for P29274 and -0.861 for P08172, highlight Chemprop(Ago)'s inability to generalize or make meaningful predictions for agonists. This failure was further corroborated by higher MSE values and lower CI scores for agonists across all tested proteins, underscoring a critical limitation in Chemprop's generalizability. In contrast, AiGPro demonstrated robust performance across both agonists and antagonists, consistently delivered high predictive accuracy and reliability across all proteins even on skewed datasets such as P08172, outperforming Chemprop models in overall generalization. pdcsm-GPCR's inability to process agonists or antagonists underscores its lack of versatility; its ability to maintain high performance across diverse ligand types makes it a versatile tool for profiling large-scale GPCRs. These results emphasize the limitations of existing models in handling mixed activity datasets and underscore the need for AiGPro's broader applicability and reliability in GPCR profiling.

Further, we also performed classification tests, the findings of which are presented in Fig. 6A, B. These findings highlight AiGPro's robust performance even on classification tasks on novel datasets. Demonstrating notably high Cohen's kappa, ROC-AUC, and MCC values for both agonist and antagonist ligands, these results affirm the reliability of AiGPro and reassure its robust performance in classification tasks. Such validation underscores its potential importance in advancing practical research and enhancing GPCR targeted drug discovery efforts.

Limitations

While AiGPro demonstrates significant advancements in predicting both agonistic and antagonistic activities across GPCRs, it has certain limitations. The model's performance relies heavily on the availability of high-quality training data. Despite our dataset being among the most comprehensive for GPCRs, it remains sparse for specific targets. This data sparsity particularly impacts the model's generalizability for underrepresented GPCR families and ligands with rare activity profiles, with agonistic ligands notably underrepresented. Although our approach addresses some challenges associated with traditional multi-task models, data imbalance remains a significant limitation. Agonist data is considerably less abundant than antagonist data, as illustrated in Fig. 1. This imbalance has resulted in higher MSE values exceeding 1.00 for proteins like Q14833 and Q16602, as shown

in Table 2, introducing biases that can affect prediction accuracy for these targets. Furthermore, as demonstrated in the case study, AiGPro may not be well-suited for single-target predictions and may underperform compared to single-task models specifically optimized for antagonistic activity.

Moreover, AiGPro does not fully account for experimental variations, such as receptor conformations from 3D structures, which can significantly influence bioactivity values. Although innovative data processing techniques were applied to reduce inconsistencies, its capacity to model complex ligand behaviors, such as partial agonism or antagonism, is not yet fully explored, indicating potential areas for further development. These challenges underscore the need to development of innovative techniques to enhance AiGPro's robustness and broader applicability.

AiGPro web service

We have developed a user-friendly web server, accessible at <https://aicadd.ssu.ac.kr/AiGPro>, to facilitate the utilization of the AiGPro models for individuals with limited coding expertise. See Fig. 7. This online platform enables users to submit a SMILES string representing their query compounds, generating a profile against 231 GPCRs. The computed results, presented as activity scores, are conveniently organized in a paginated table, with each page displaying 10 predictions encompassing both antagonist and agonist compounds, and can be downloaded in CSV file format for further analysis. The tool is designed to determine the nature of given small molecules, categorizing them as agonists, antagonists, or inactive compounds for GPCR proteins.

The platform's efficient processing speed and user-friendly interface make it invaluable for drug screening and design endeavors.

Conclusion

This study presents AiGPro, a novel bi-directional multi-head cross-attention incorporating a multi-scale content aggregation-based model, leveraging the self-attention mechanism and dilated convolution. Our proposed framework facilitates the comprehensive exploration and learning of both intra and intermolecular features of GPCRs and ligands, thereby enhancing generalizability for accurate prediction of bioactivity values for both agonist (EC_{50}) and antagonist (IC_{50}) activities.

GPCRs play a pivotal role in human pathophysiology, making them a prime target for drug discovery. However, the complexity of GPCRs and the scarcity of high-quality data have led to limited applicability of prior ML approaches. AiGPro overcomes these challenges,

demonstrating exceptional performance and applicability domain across 231 GPCRs, thus establishing itself as the first-in-class method for GPCR profiling, setting new benchmarks in accuracy and efficacy for identifying and eliminating off-targets. This advancement holds promise for accelerating GPCR drug development by facilitating high throughput screening, compound evaluation, prioritization, and prediction of activity profiles.

Our results demonstrated that an innovative model could predict both agonist and antagonist bioactivity values of GPCR ligands with superior performance compared to complex ensemble models, eliminating the need for ensemble models. Further, we have developed and deployed an end-to-end platform accessible at <https://aicadd.ssu.ac.kr/AiGPro>, enabling convenient access to AiGPro models for the identification of off-targets against GPCRs, thereby offering scalable, rapid, and precise profiling of small molecules. The community can leverage the user-friendly web server AiGPro to enrich molecule libraries for screening purposes and facilitate rational GPCR ligand design.

Supplementary Information

The online version contains supplementary material available at <https://doi.org/10.1186/s13321-024-00945-7>.

Additional file 1.
Additional file 2.
Additional file 3.
Additional file 4.

Acknowledgements

The subject is supported by KREONET (Korean Research Environment Open NETWORK), which is managed and operated by KISTI (Korean Institute of Science and Technology Information). We thank the National Institute for International Education (NIIED), Government of the Republic of Korea, for the Global Korean Scholarship to R.B. This research was supported by Basic Science Research Program through the National Research Foundation of Korea (NRF) funded by the Ministry of Education (2021R1A6A1A10044154).

Author contributions

Experiments, coding, writing, web server, database development, and maintenance were conducted by R.B under the supervision of K.H.C, with conceptualization by J.M.S and K.H.C. S.H.M helped to build the web server. All authors reviewed the manuscript.

Data availability

AiGPro predictive models have been made available via a freely accessible and easy-to-use web server at <https://aicadd.ssu.ac.kr/AiGPro>. Code and dataset used to develop the models can be accessed from Glass (<https://zhanggroup.org/GLASS/>) and GPCRdb (<https://gpcrdb.org/>) and Code (<https://github.com/Chemoinformatics/AiGPro>) and models weights can be downloaded from (<https://aicadd.ssu.ac.kr/download>). No datasets were generated or analysed during the current study.

Declarations

Competing interests

The authors declare no competing interests.

Author details

¹School of Systems Biomedical Science, Soongsil University, 369 Sangdo-ro, Dongjak-gu, 06978 Seoul, Republic of Korea. ²AzothBio, Rm. DA724 Hyundai Knowledge Industry Center, Hanam-si, Gyeonggi-do, Republic of Korea.

Received: 4 August 2024 Accepted: 27 December 2024

Published online: 29 January 2025

References

- Liu N, Wang Y, Li T, Feng X (2021) G-protein coupled receptors (GPCRs): signaling pathways, characterization, and functions in insect physiology and toxicology. *Int J Mol Sci*. <https://doi.org/10.3390/IJMS22105260>
- Yang D, Zhou Q, Labroska V et al (2021) G protein-coupled receptors: structure- and function-based drug discovery. *Signal Transduct Target Ther* 1(6):1–27. <https://doi.org/10.1038/s41392-020-00435-w>
- Wong TS, Li G, Li S et al (2023) G protein-coupled receptors in neurodegenerative diseases and psychiatric disorders. *Signal Transduct Target Ther* 1(8):1–57. <https://doi.org/10.1038/s41392-023-01427-2>
- Velloso JPL, Kovacs AS, Pires DEV, Ascher DB (2024) AI-driven GPCR analysis, engineering, and targeting. *Curr Opin Pharmacol* 74:102427. <https://doi.org/10.1016/J.COPH.2023.102427>
- Hauser AS, Attwood MM, Rask-Andersen M et al (2017) Trends in GPCR drug discovery: new agents, targets and indications. *Nat Rev Drug Discov* 12(16):829–842. <https://doi.org/10.1038/nrd.2017.178>
- Sriram K, Insel PA (2018) G protein-coupled receptors as targets for approved drugs: how many targets and how many drugs? *Mol Pharmacol* 93:251–258. <https://doi.org/10.1124/MOL.117.111062/-DC1>
- Fribourg M, Moreno JL, Holloway T et al (2011) Decoding the signaling of a GPCR heteromeric complex reveals a unifying mechanism of action of antipsychotic drugs. *Cell* 147:1011–1023. <https://doi.org/10.1016/j.cell.2011.09.055>
- Schmid CL, Streicher JM, Meltzer HY, Bohn LM (2014) Clozapine Acts as an Agonist at Serotonin 2A Receptors to Counter MK-801-Induced Behaviors through a β Arrestin2-Independent Activation of Akt. *Neuropsychopharmacology* 8(39):1902–1913. <https://doi.org/10.1038/npp.2014.38>
- Jendryka M, Palchadhuri M, Ursu D et al (2019) Pharmacokinetic and pharmacodynamic actions of clozapine-N-oxide, clozapine, and compound 21 in DREADD-based chemogenetics in mice. *Sci Rep* 9(1):1–14. <https://doi.org/10.1038/s41598-019-41088-2>
- Cheng L, Xia F, Li Z et al (2023) Structure, function and drug discovery of GPCR signaling. *Mol Biomed* 4:46. <https://doi.org/10.1186/S43556-023-00156-W>
- Oprea TI, Bologa CG, Brunak S et al (2018) Unexplored therapeutic opportunities in the human genome. *Nat Rev Drug Discov* 5(17):317–332. <https://doi.org/10.1038/nrd.2018.14>
- Congreve M, de Graaf C, Swain NA, Tate CG (2020) Impact of GPCR structures on drug discovery. *Cell* 181:81–91. <https://doi.org/10.1016/J.CELL.2020.03.003>
- Chen Z, Ren X, Zhou Y, Huang N (2024) Exploring structure-based drug discovery of GPCRs beyond the orthosteric binding site. *hLife*. <https://doi.org/10.1016/J.HLIFE.2024.01.002>
- Kooistra AJ, Mordalski S, Pándy-Szekeres G et al (2021) GPCRdb in 2021: integrating GPCR sequence, structure and function. *Nucleic Acids Res* 49:D335–D343. <https://doi.org/10.1093/NAR/GKAA1080>
- Pándy-Szekeres G, Caroli J, Mamyrbekov A et al (2023) GPCRdb in 2023: state-specific structure models using AlphaFold2 and new ligand resources. *Nucleic Acids Res* 51:D395–D402. <https://doi.org/10.1093/NAR/GKAC1013>
- Chan WKB, Zhang Y (2020) Virtual screening of human class-A GPCRs using ligand profiles built on multiple ligand-receptor interactions. *J Mol Biol* 432:4872. <https://doi.org/10.1016/J.JMB.2020.07.003>
- Ahmed M, Hasani HJ, Kalyaanamoorthy S, Barakat K (2021) GPCR_Ligand-Classify.py; a rigorous machine learning classifier for GPCR targeting compounds. *Sci Rep* 11:9510. <https://doi.org/10.1038/S41598-021-88939-5>
- Wang K, Zhou R, Tang J, Li M (2023) GraphscoreDTA: optimized graph neural network for protein–ligand binding affinity prediction. *Bioinformatics*. <https://doi.org/10.1093/BIOINFORMATICS/BTAD340>

19. Yousefi N, Yazdani-Jahromi M, Tayebi A et al (2023) BindingSite-AugmentedDTA: enabling a next-generation pipeline for interpretable prediction models in drug repurposing. *Brief Bioinform* 24:1–13. <https://doi.org/10.1093/BIB/BBAD136>
20. Yazdani-Jahromi M, Yousefi N, Tayebi A et al (2022) AttentionSiteDTI: an interpretable graph-based model for drug-target interaction prediction using NLP sentence-level relation classification. *Brief Bioinform* 23:1–14. <https://doi.org/10.1093/BIB/BBAC272>
21. Park H, Brahma R, Shin JM, Cho KH (2022) Prediction of human cytochrome P450 inhibition using bio-selectivity induced deep neural network. *Bull Korean Chem Soc* 43:261–269. <https://doi.org/10.1002/BKCS.12445>
22. Park H, Hong S, Lee M et al (2023) AiKPro: deep learning model for kinome-wide bioactivity profiling using structure-based sequence alignments and molecular 3D conformer ensemble descriptors. *Sci Rep* 1(13):1–12. <https://doi.org/10.1038/s41598-023-37456-8>
23. Brahma R, Shin JM, Cho KH (2023) KinScan: AI-based rapid profiling of activity across the kinome. *Brief Bioinform*. <https://doi.org/10.1093/BIB/BBAD396>
24. Seo S, Choi J, Ahn SK et al (2018) Prediction of GPCR-ligand binding using machine learning algorithms. *Comput Math Methods Med*. <https://doi.org/10.1155/2018/6565241>
25. Karimi S, Ahmadi M, Goudarzi F, Ferdousi R (2020) A computational model for GPCR-ligand interaction prediction. *J Integr Bioinform* 18:155–165. https://doi.org/10.1515/JIB-2019-0084/DOWNLOADASSET/SUPPL/J_JIB-2019-0084_SUPPL.XLSX
26. Yamane H, Ishida T (2023) Helix encoder: a compound-protein interaction prediction model specifically designed for class A GPCRs. *Front Bioinform* 3:1193025. <https://doi.org/10.3389/FBINF.2023.1193025/BIBTEX>
27. Remington JM, McKay KT, Beckage NB et al (2023) GPCR LigNet: rapid screening for GPCR active ligands using machine learning. *J Comput Aided Mol Des* 37:147–156. <https://doi.org/10.1007/S10822-023-00497-2/METRICS>
28. Cai T, Abbu KA, Liu Y, Xie L (2022) DeepREAL: a deep learning powered multi-scale modeling framework for predicting out-of-distribution ligand-induced GPCR activity. *Bioinformatics* 38:2561–2570. <https://doi.org/10.1093/BIOINFORMATICS/BTAC154>
29. Wu Z, Cheng F, Li J et al (2017) SDTNBf: an integrated network and cheminformatics tool for systematic prediction of drug-target interactions and drug repositioning. *Brief Bioinform* 18:333–347. <https://doi.org/10.1093/BIB/BBW012>
30. Oh J, Ceong H, Na D, Park C (2022) A machine learning model for classifying G-protein-coupled receptors as agonists or antagonists. *BMC Bioinform* 23:1–10. <https://doi.org/10.1186/S12859-022-04877-7/TABLES/2>
31. Chu Y, Shan X, Chen T et al (2021) DTI-MLCD: predicting drug-target interactions using multi-label learning with community detection method. *Brief Bioinform* 22:1–15. <https://doi.org/10.1093/BIB/BBAA205>
32. Goßen J, Ribeiro RP, Bier D et al (2023) AI-based identification of therapeutic agents targeting GPCRs: introducing ligand type classifiers and systems biology. *Chem Sci* 14:8651–8661. <https://doi.org/10.1039/D3SC02352D>
33. Merighi S, Borea PA, Varani K et al (2022) A2A adenosine receptor antagonists in neurodegenerative diseases. *Curr Med Chem* 29:4138. <https://doi.org/10.2174/0929867328666211129122550>
34. Al-Attraqchi OHA, Attimarad M, Venugopala KN et al (2019) Adenosine A2A receptor as a potential drug target—current status and future perspectives. *Curr Pharm Des* 25:2716–2740. <https://doi.org/10.2174/1381612825666190716113444>
35. Jiménez-Rosés M, Morgan BA, Jimenez Sigstad M et al (2022) Combined docking and machine learning identify key molecular determinants of ligand pharmacological activity on β_2 adrenoceptor. *Pharmacol Res Perspect*. <https://doi.org/10.1002/PRP2.994>
36. Xu H, Zhang B, Liu Q (2023) Deep learning-based classification model for GPR151 activator activity prediction. *BMC Bioinform*. <https://doi.org/10.1186/S12859-023-05369-Y>
37. Wu J, Liu B, Chan WKB et al (2019) Precise modelling and interpretation of bioactivities of ligands targeting G protein-coupled receptors. *Bioinformatics* 35:i324–i332. <https://doi.org/10.1093/BIOINFORMATICS/BTZ336>
38. Wu J, Zhang Q, Wu W et al (2018) WDL-RF: predicting bioactivities of ligand molecules acting with G protein-coupled receptors by combining weighted deep learning and random forest. *Bioinformatics* 34:2271. <https://doi.org/10.1093/BIOINFORMATICS/BTY070>
39. Sakai M, Nagayasu K, Shibui N et al (2021) Prediction of pharmacological activities from chemical structures with graph convolutional neural networks. *Sci Rep* 1(11):1–14. <https://doi.org/10.1038/s41598-020-80113-7>
40. Velloso JPL, Ascher DB, Pires DEV (2021) pdCSM-GPCR: predicting potent GPCR ligands with graph-based signatures. *Bioinform Adv*. <https://doi.org/10.1093/BIOADV/VBAC031>
41. Huang WC, Lin WT, Hung MS et al (2024) Decrypting orphan GPCR drug discovery via multitask learning. *J Cheminform* 16:1–11. <https://doi.org/10.1186/S13321-024-00806-3/FIGURES/6>
42. Bhatnagar R, Sardar S, Beheshti M, Podichetty JT (2022) How can natural language processing help model informed drug development?: a review. *JAMIA Open* 5:1–14. <https://doi.org/10.1093/JAMIAOPEN/OOAC043>
43. Hu Z, Liu W, Zhang C et al (2023) SAM-DTA: a sequence-agnostic model for drug-target binding affinity prediction. *Brief Bioinform* 24:1–15. <https://doi.org/10.1093/BIB/BBAC533>
44. Huang Z, Zhang P, Deng L (2023) DeepCoVDR: deep transfer learning with graph transformer and cross-attention for predicting COVID-19 drug response. *Bioinformatics* 39:i475–i483. <https://doi.org/10.1093/BIOINFORMATICS/BTAD244>
45. Thakur A, Kumar A, Sharma V, Mehta V (2022) PIC50: an open source tool for interconversion of PIC50 values and IC50 for efficient data representation and analysis. *bioRxiv*. <https://doi.org/10.1101/2022.10.15.512366>
46. RDKit. <https://www.rdkit.org/>
47. Vaswani A, Shazeer N, Parmar N, et al (2017) Attention Is All You Need. *Adv Neural Inf Process Syst* 2017–December:5999–6009
48. Chicco D, Jurman G (2020) The advantages of the Matthews correlation coefficient (MCC) over F1 score and accuracy in binary classification evaluation. *BMC Genomics* 21:1–13. <https://doi.org/10.1186/S12864-019-6413-7/TABLES/5>
49. Dwomoh L, Tejada GS, Tobin AB (2022) Targeting the M1 muscarinic acetylcholine receptor in Alzheimer's disease. *Neuronal Signal* 6:20210004. <https://doi.org/10.1042/NS20210004>
50. Brown AJH, Bradley SJ, Marshall FH et al (2021) From structure to clinic: design of a muscarinic M1 receptor agonist with potential to treatment of Alzheimer's disease. *Cell* 184:5886–5901.e22. <https://doi.org/10.1016/J.CELL.2021.11.001>
51. Shirey JK, Brady AE, Jones PJ et al (2009) A selective allosteric potentiator of the m1 muscarinic acetylcholine receptor increases activity of medial prefrontal cortical neurons and restores impairments in reversal learning. *J Neurosci* 29:14271. <https://doi.org/10.1523/JNEUROSCI.3930-09.2009>
52. Rowe WB, O'Donnell JP, Pearson D et al (2003) Long-term effects of BIBN-99, a selective muscarinic M2 receptor antagonist, on improving spatial memory performance in aged cognitively impaired rats. *Behav Brain Res* 145:171–178. [https://doi.org/10.1016/S0166-4328\(03\)00116-5](https://doi.org/10.1016/S0166-4328(03)00116-5)
53. Poulin B, Butcher A, McWilliams P et al (2010) The M3-muscarinic receptor regulates learning and memory in a receptor phosphorylation/arrestin-dependent manner. *Proc Natl Acad Sci USA* 107:9440–9445. <https://doi.org/10.1073/PNAS.0914801107/-/DCSUPPLEMENTAL>
54. Heid E, Greenman KP, Chung Y, et al (2024) Chemprop: A Machine Learning Package for Chemical Property Prediction. *J Chem Inf Model* 64:9–17. <https://doi.org/10.1021/ACS.JCIM.3C01250>

Publisher's Note

Springer Nature remains neutral with regard to jurisdictional claims in published maps and institutional affiliations.